Supplementary Information (SI) for Physical Chemistry Chemical Physics.
This journal is © the Owner Societies 2024

Supporting Information

Evolution of Electronic Structure and Optical Properties of Naphthalenediimide Dithienylvinylene (NDI-TVT) Polymer as a Function of Reduction Level: A Density Functional Theory Study

Sushri Soumya Jena, Mohit Garg, and Sarbani Ghosh*

Department of Chemical Engineering, Birla Institute of Technology and Science (BITS), Pilani Campus, Vidya Vihar, Pilani, 333031, Rajasthan, India

*sarbani.ghosh@pilani.bits-pilani.ac.in

Section-1: Model and Methods

We have optimized the charge-neutral/pristine (Q=0) and the negatively- doped PNDI-TVT to obtain a minimum-energy structure at each reduction level, viz., Q= -1 (C_{red}= 20%), Q= -2 (C_{red}= 40%), Q= -3 (C_{red}= 60%), Q= -4 (C_{red}= 80%), Q= -5 (C_{red}= 100%), Q= -6 (C_{red}= 120%) and Q= -10 (C_{red}= 200%), and studied the effect of doping levels on the (opto)electronic properties. In this study, we have used the Berny geometry optimization algorithm[1]. The Berny algorithm is a quasi-Newton method that is robust and effective for most molecular systems and refined with rational function optimization. During the geometry optimization, the threshold values of average force and average changes over distance were fixed to the value of ~1×10-2 eV/Å and ~6.3×10-4 Å, respectively. The SCF stopping criteria we have used for all DFT calculations is 2x10-8 eV or 10-9 Hartree. We have used the Ultra-fine integration grids for the DFT calculations. To optimize the ground state of the charge-neutral (Q=0) and the singlet state of the negatively charged chain with an even number of charges per chain (Q= -2, -4, and -6), we performed the spin-restricted DFT calculations. The ground-state calculations with an odd number of electrons (Q= -1, -3, and -5) and for the triplet and quintet states, calculations of the polymer with an even number of electrons were carried out using the spin unrestricted DFT calculations. During the open-shell calculation of unrestricted spin states, especially in the case of high spin multiplicity, there are possibilities of spin contamination, which in turn can affect the TDDFT results[2]. Finding any significant spin contamination in DFT calculations is less common, even when unrestricted Kohn-

Sham orbitals are used[3]. A low value of spin contamination indicates that the wave function closely approximates a pure spin state, and typically, a contamination value below 10% is considered negligible[3]. The spin contamination calculated as [<S2> - s(s+1)] for the unrestricted high spin states yield values in the range of $10^{-3,}$ suggesting that our calculations provide correct solutions for the maximum Sz components[3,4,5] of the high spin multiplicities, see Table S3. The electron spin/charge distribution on individual NDI units is obtained by integrating over the spin/charge density of the individual NDI units within the NDI-TVT oligomeric chain. To plot the UV-vis absorption spectra, we used a Gaussian line shape with a full width at half maximum (FWHM) value of 0.15 eV to achieve phenomenological broadening.

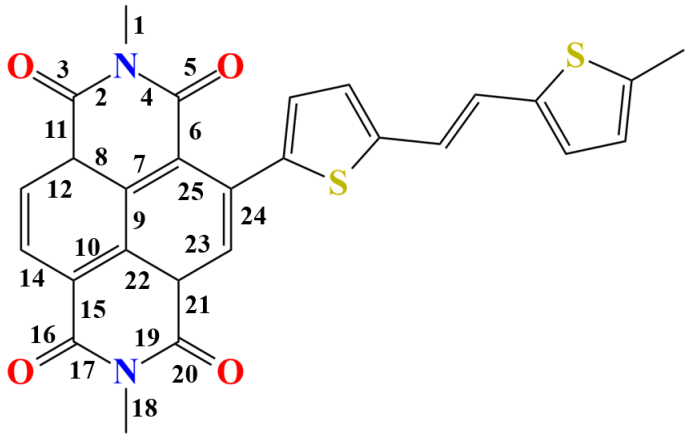

Figure S1: The bond numbers of the NDI unit, which are used to calculate the bond-length alteration, are marked.

Section-2: Additional Properties calculated at ωB97XD/6-31+G(d) (in gas phase)

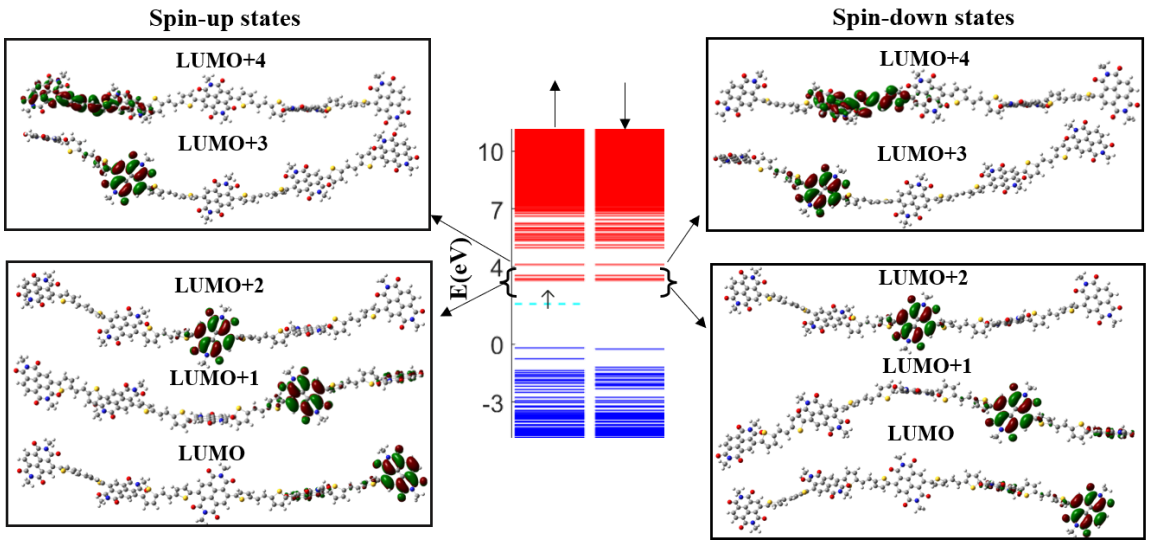

Figure S2. Band diagram and electron density distributions of HOMO and some lower lying HOMOs and LUMO and some higher lying LUMOs of doped NDI-TVT (Q= -1). Empty electronic states in the conduction band are visualized for the doped states and both conduction band and valence band electronic states are visualized for the undoped states in gas phase.

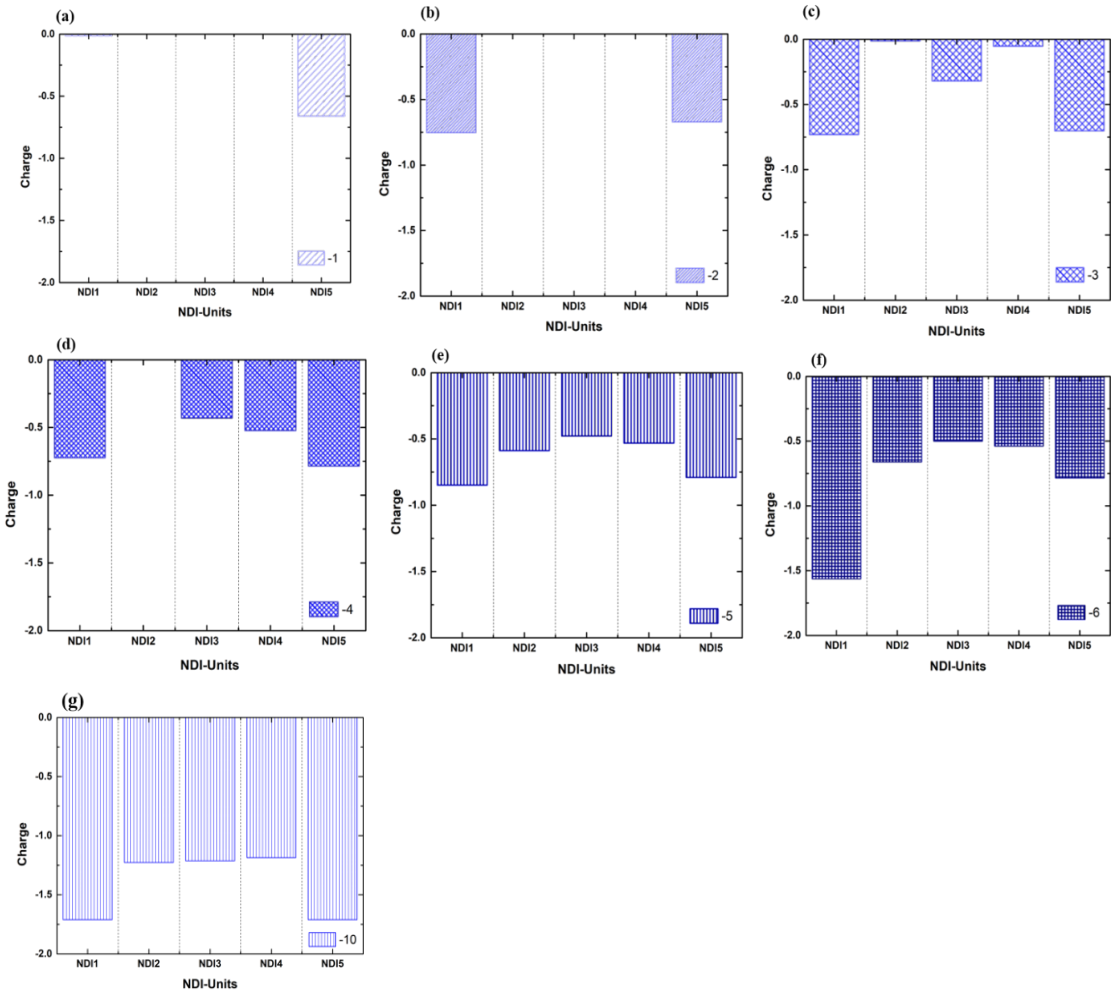

Figure S3: The charge distribution on different NDI units within the NDI-TVT polymer chain showing the distinct distribution of charge at various doped levels from Q= -1 to -6, -10 in the gas phase.

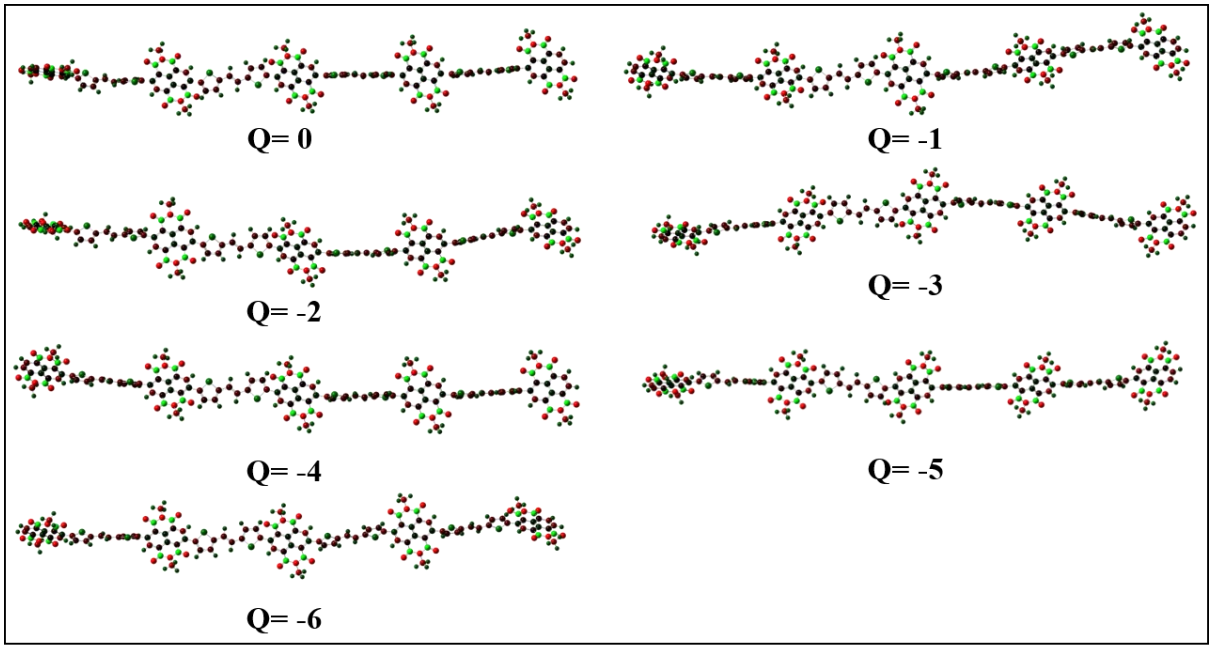

Figure S4: Charge distribution of undoped and doped NDI-TVT polymer in the gas phase.

Section-3: Effect of Diffuse Function

Table.S1: Spin Multiplicity (M) and Total Spin (S) of the NDI-TVT oligomeric chain using both basis set 6-31+G and 6-31G for pristine and different charged states from Q= -1 to -6 and -10 in gas and solvent phase for the lowest energy state.

Charges(Q)	Gas phase				Solvent phase	
	Spin Multiplicity (M)		Total Spin (S)		Spin Multiplicity(M)	Total Spin (S)
	6-31G+(d)	6-31G (d)	6-31G+(d)	6-31G (d)	6-31G+(d)	6-31G+(d)
0	Singlet(1)	Singlet(1)	0	0	Singlet(1)	0
-1	Double(2)	Double(2)	0.5	0.5	Double(2)	0.5
-2	Triplet(3)	Triplet(3)	1	1	Triplet(3)	1
-3	Doublet(2)	Doublet(2)	0.5	0.5	Quartet(4)	1.5
-4	Triplet(3)	Triplet(3)	1	1	Pentet(5)	2
-5	Doublet(2)	Doublet(2)	0.5	0.5	Sextet(6)	2.5
-6	Triplet(3)	Triplet(3)	1	1	Pentet(5)	2
-10	Singlet(1)	Singlet(1)	0	0	Singlet(1)	0

3.1. Electronic structures calculated at a lower basis set without diffuse basis functions (+) (in the gas phase)

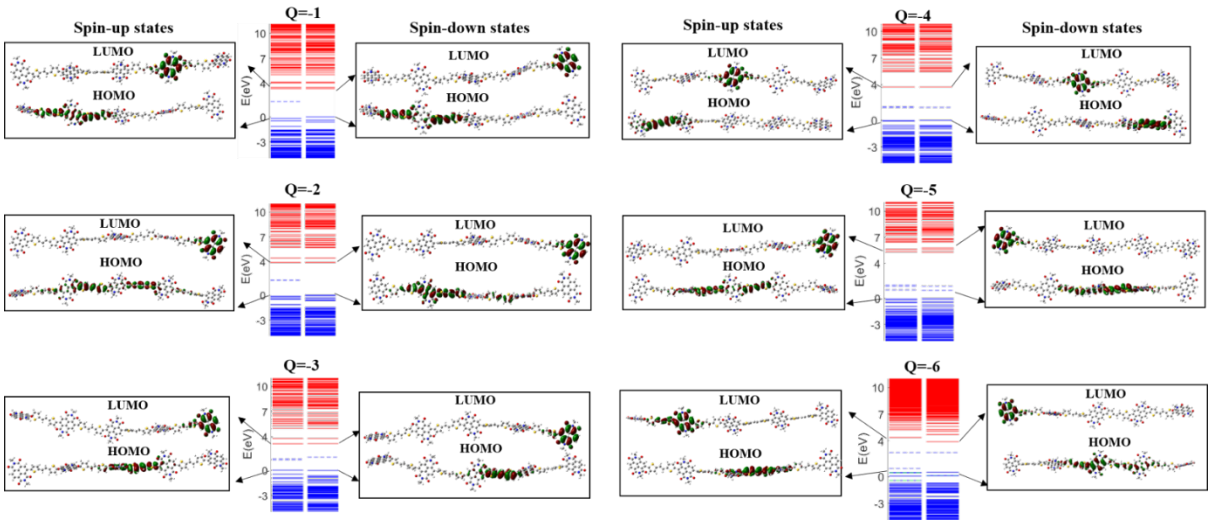

Figure S5: Band diagrams and molecular orbitals of HOMO (highest occupied molecular orbital) and LUMO (lowest unoccupied molecular orbital) of NDI-TVT polymer at different charged states, Q=-1 to -6, in the gas phase.

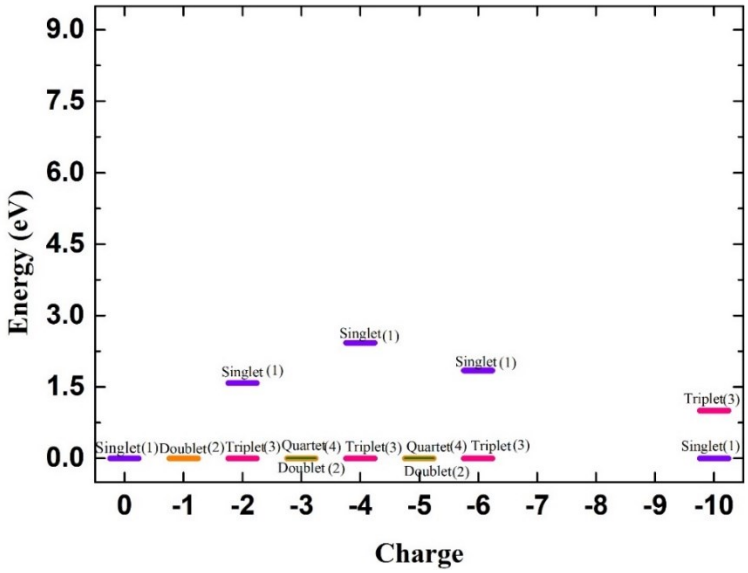

Figure S6: Total energy of the NDI-TVT chain of different spin states, singlet (1), doublet (2), triplet (3), quartet (4) for pristine and different charged states from Q= -1 to -6 and 10 in the gas phase.

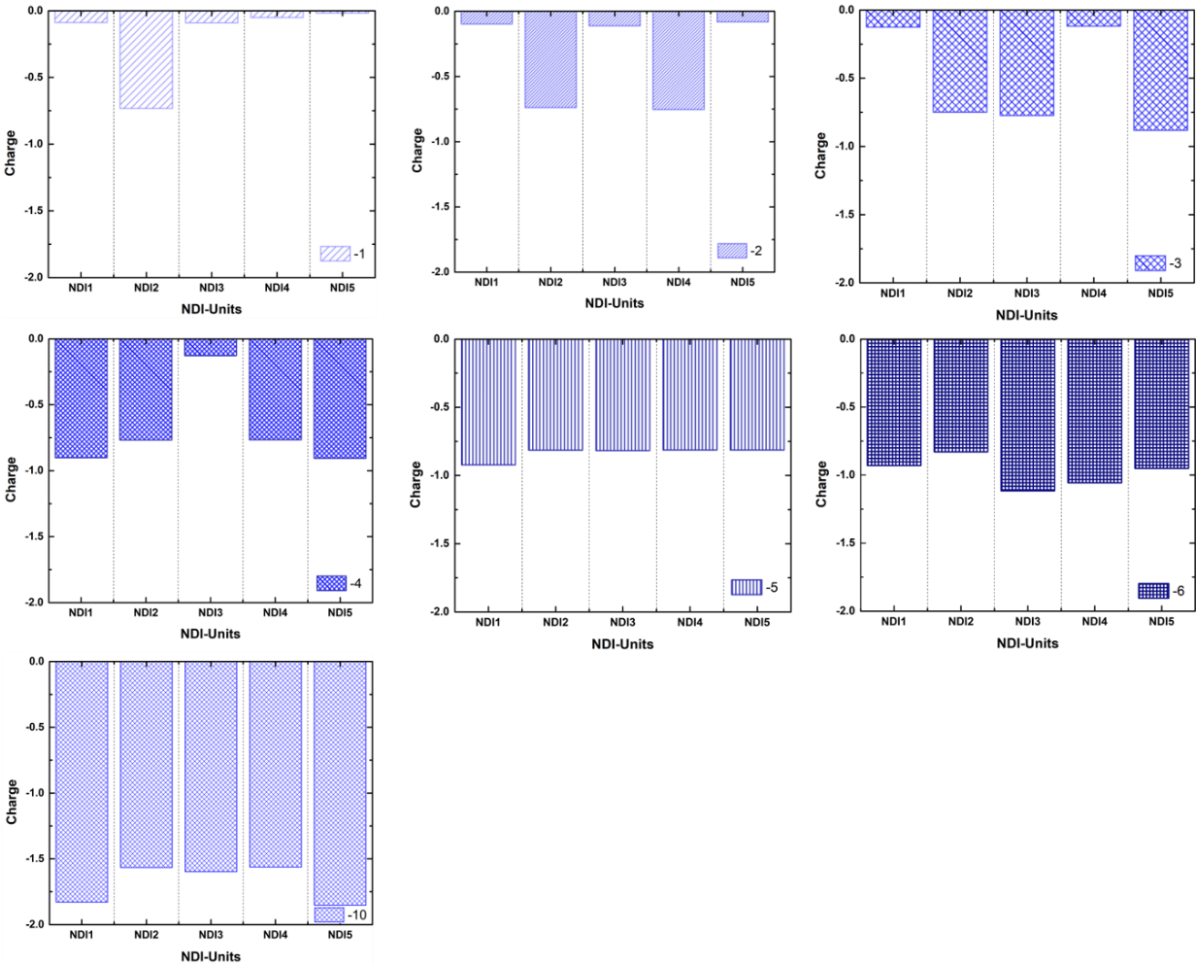

Figure S7: The charge distribution on different NDI-Units within the NDI-TVT polymer chain at various doped levels from Q= -1 to -6 and -10 in the gas phase.

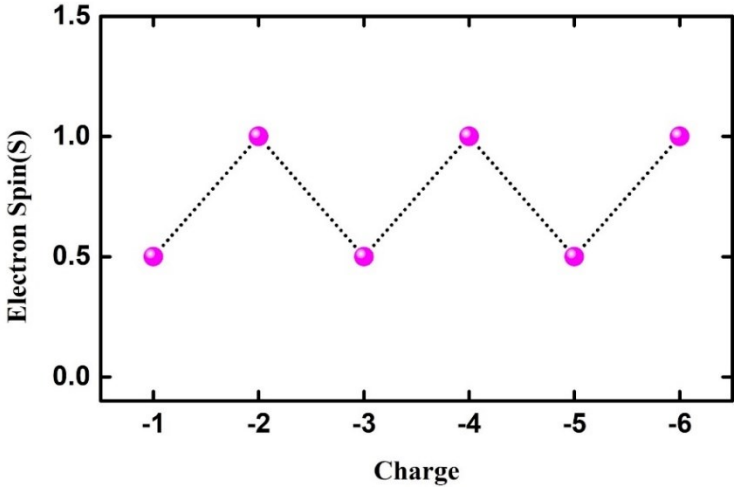

Figure S8: Total electron spin (S) of NDI-TVT chain at different doping levels in gas phase.

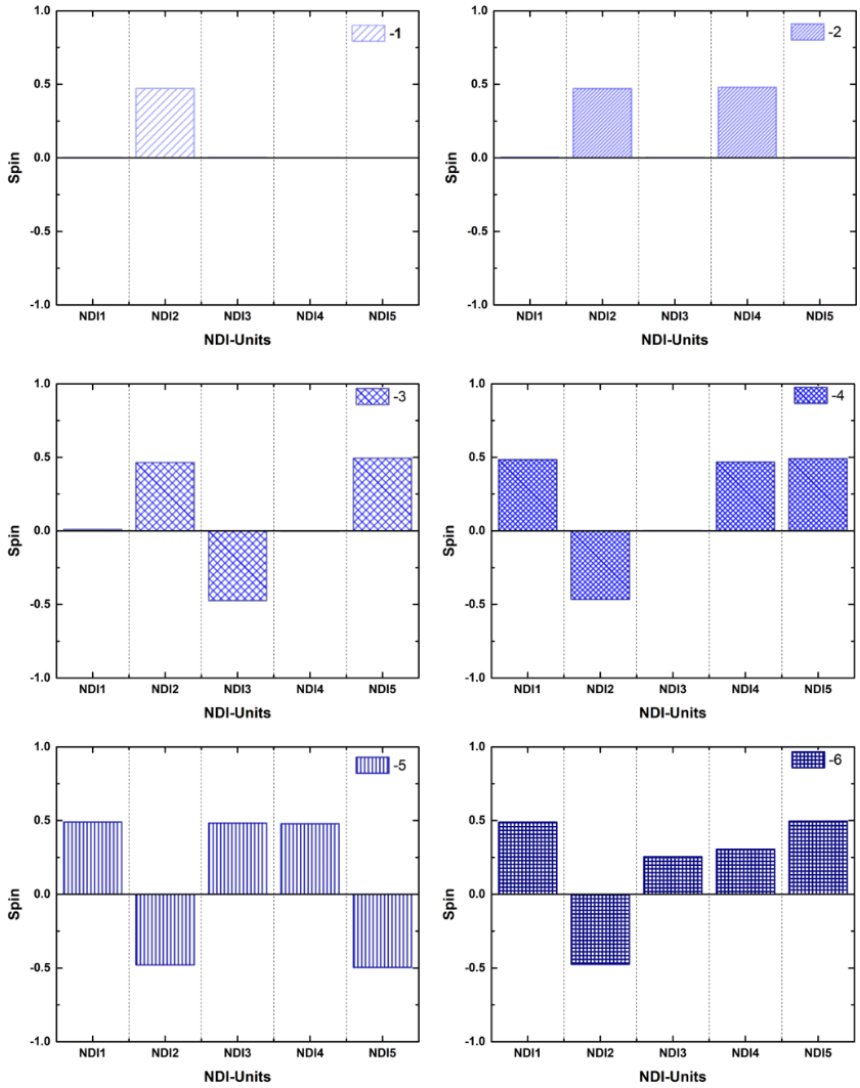

Figure S9: The electronic spin distribution on individual NDI-Units within the NDI-TVT polymer chain showing distinct spin states at all the reduction levels in gas phase.

3.2. Electronic structure and optical properties of NDI-TVT polymer with diffuse basis functions (+) (in gas phase)

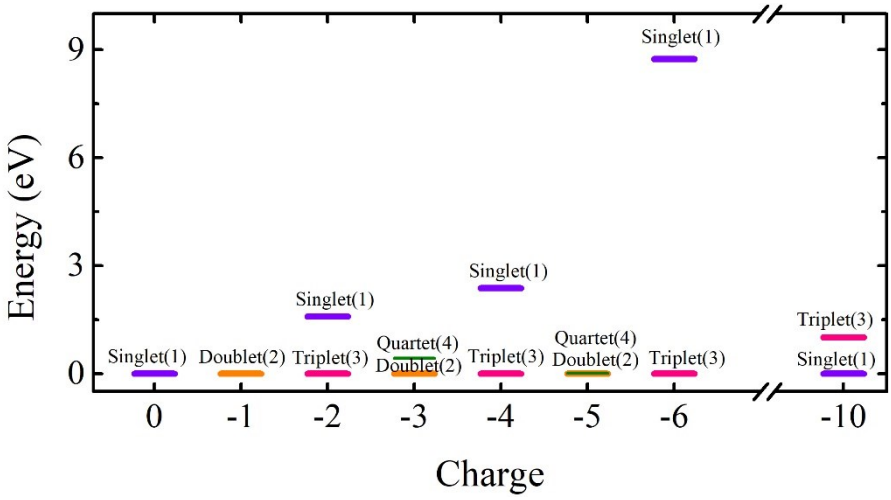

Figure S10: Total energy of the NDI-TVT chain of different spin states, singlet (1), doublet (2), triplet (3), quartet (4) for pristine and different charged states from Q= -1 to -6 and 10 in gas phase.

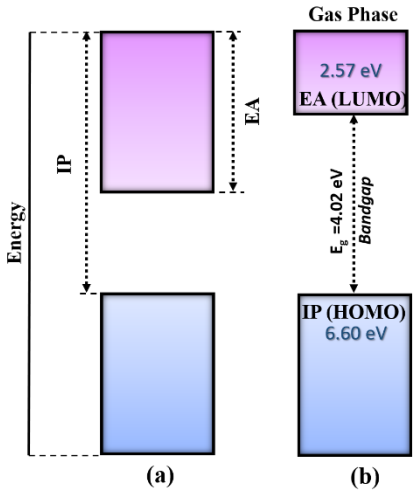

Figure S11: (a) Schematic representation of the definition of the ionization potential (IP) and the electron affinity (EA), (b) IE and EA of NDI-TVT polymer in the gas phase.

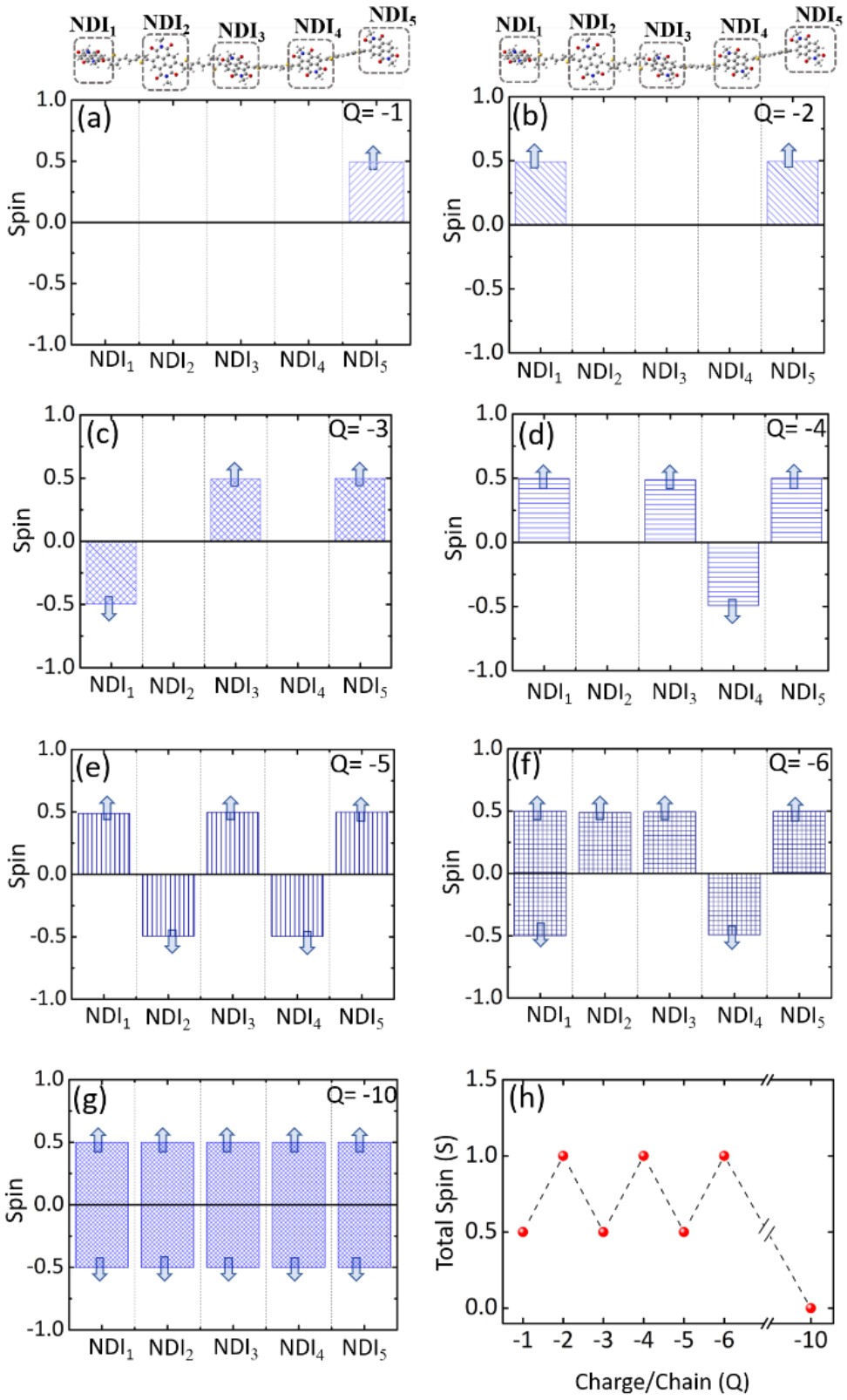

Figure S12: The electronic spin distribution on individual NDI-units within the NDI-TVT polymer chain showing distinct spin states at all the reduction levels (a) Q= -1, (b) Q=-2, (C) Q=-3, (d) Q=-4, (e) Q=-5, (f) Q=-6, and (g) Q= -10. (h) The total spin of the PNDI-TVT chain at different charged states in the gas phase.

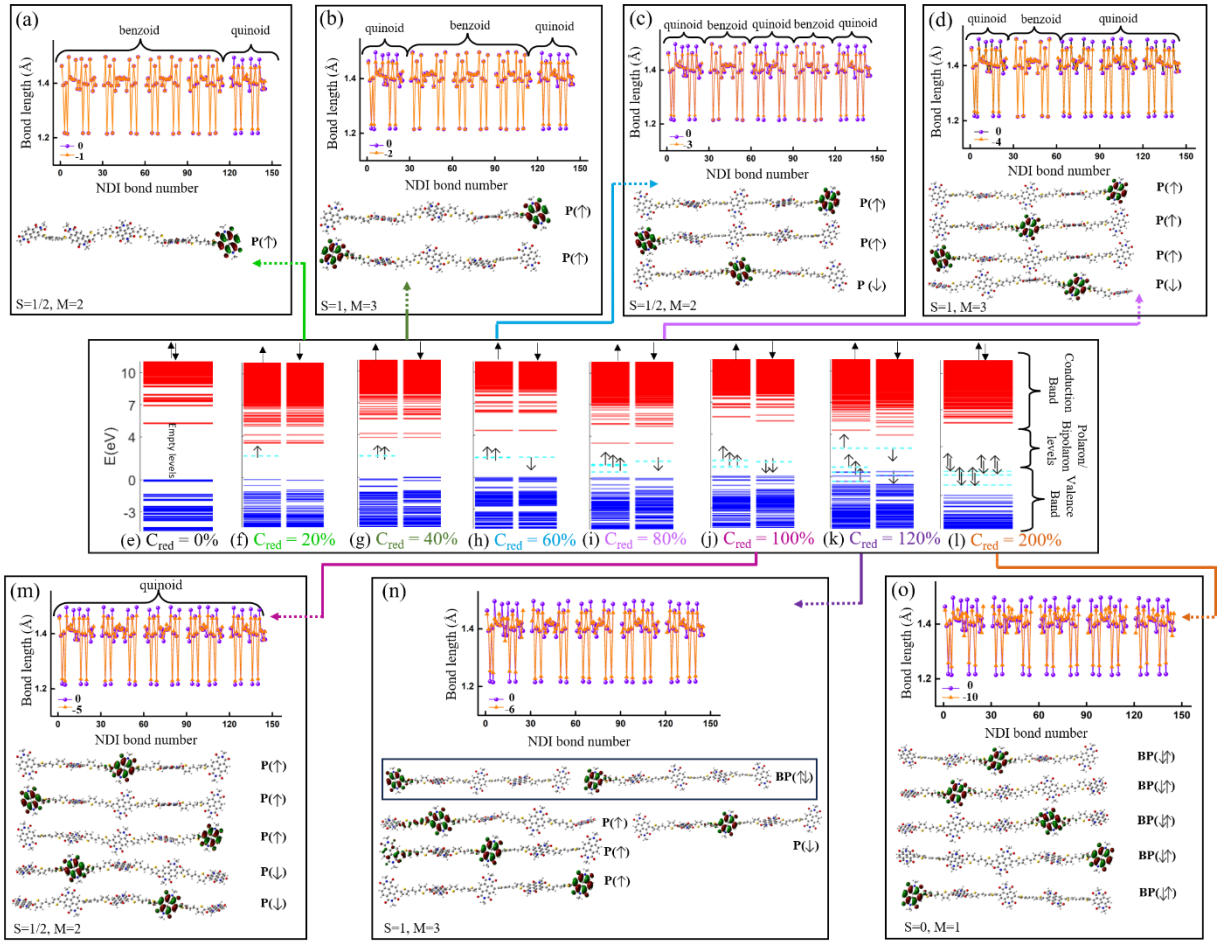

Figure S13. (In gas phase) Molecular orbitals of polaron/bipolaron states along with bond-length alteration of NDI moieties for all the doped states in the gas phase (a) Q= -1 (C_{red}=20%), (b) Q= -2 (C_{red}=40%), (c) Q= -3 (C_{red}=60%), (d) Q= -4 (C_{red}=80%), (m) Q= -5 (C_{red}=100%), (n) Q= -6 (C_{red}=120%), (o) Q=-10 (C_{red}=200%). Band diagrams of (e) undoped PNDI-TVT (Q= 0) and (f-l) doped PNDI-TVT. Empty electronic levels in the conduction band are plotted as red lines, occupied electronic levels in the valence band are plotted as blue lines, and the occupied polaron, polaron pairs/bipolaron are plotted as cyan dotted lines. Up- and down arrows indicate the spin-up and spin-down states, respectively. S indicates the total spin, and M indicates the spin multiplicity.

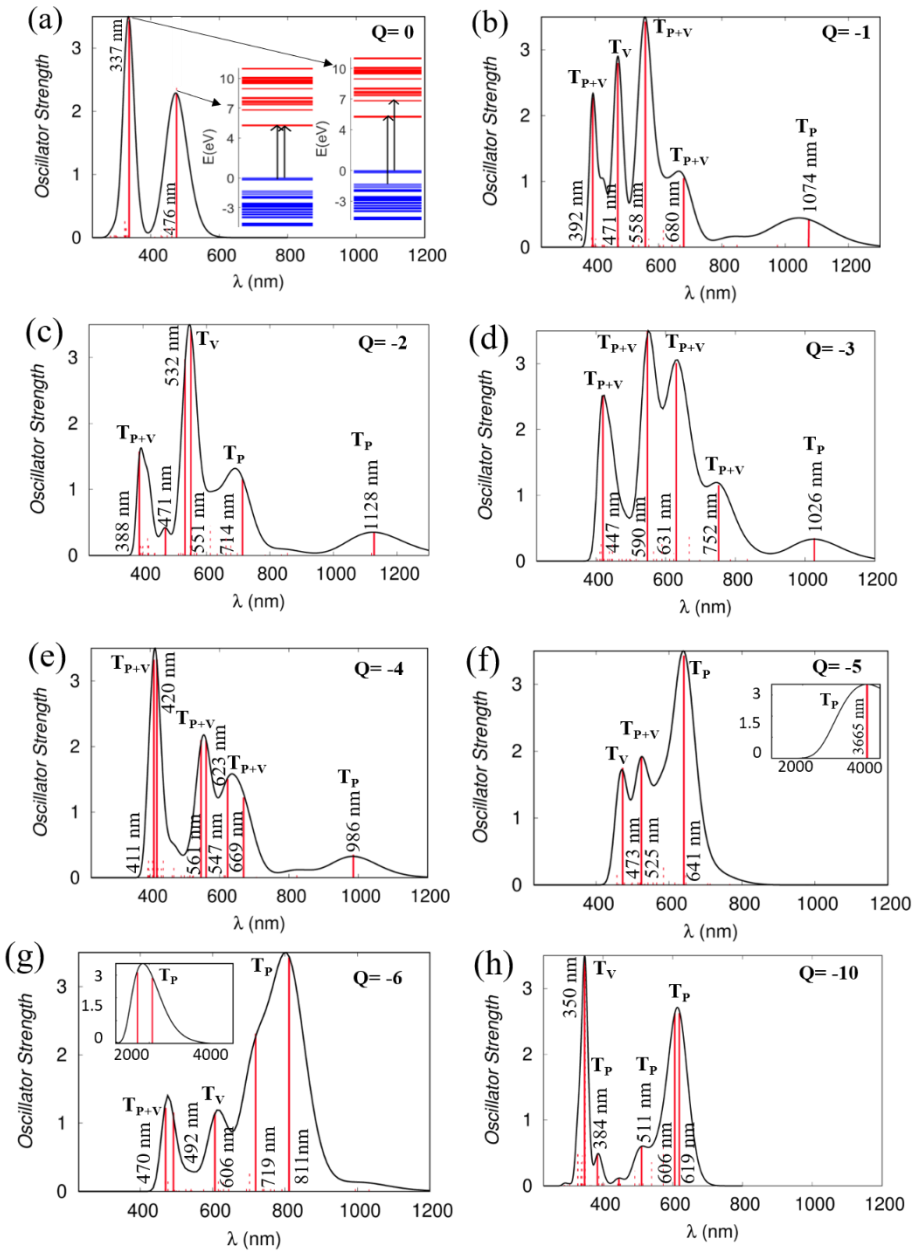

Figure S14. (a) UV vis/NIR absorption spectra of neutral NDI-TVT chain with the corresponding electronic transitions in the gas phase. (b)-(h) UV vis/NIR absorption spectra of doped NDI-TVT chain at various doped states from Q = -1 to -10 in gas phase.

Section-4: Properties of NDI-TVT Polymer Calculated using the Optimized Functional/basis-set, ωB97XD/6-31+G(d) in Solvent Phase

Table.S2: Wavelengths, coefficients, corresponding orbitals, and transition calculated for NDI-TVT in the solvent phase for pristine and different doped states from Q = -1 to -6 and Q=-10.

Charges (Q)	Wavelength (λ)	Coefficients	Corresponding Orbitals	Transitions
0	1. 460 nm, 2. 450 nm — $Peak_1$	1. 0.45281 2. 0.3042	572 → 573 571 → 573 — LUMO = 573	
	3. 343 nm, 4. 332 nm — $Peak_2$	3. 0.21293, 0.19408 4. 0.23421, 0.21237, 0.18022	560 → 575, 562 → 573 560 → 575 572 → 580, 570 → 578 — HOMO = 572	
-1	1. 617 nm — $Peak_1$	1. 0.87643(α)	572 → 580 — LUMO (α) =574, HOMO (α) =573	T_P
	2. 460 nm, 3. 433 nm — $Peak_2$	2. 0.24138(α), 0.34520(β), 0.25094(β) 3. 0.40956(α), 0.37151(β)	572 → 575, 572 → 574, 572 → 575 573 → 595, 573 → 575 — LUMO (β) =573	T_V
	4. 383 nm — $Peak_3$	4. 0.40766(β)	572 → 577 — HOMO (β) =572	T_V
-2	1. 617 nm — $Peak_1$	1. 0.71423(α)	574 → 586 — LUMO (α) =575, HOMO (α) =574	T_P
	2. 459 nm, 3. 435 nm — $Peak_2$	2. 0.26912(α), 0.26107(α), 0.39927(β) 3. 0.58607, 0.34183	573 → 576, 572 → 576, 571 → 574 573 → 593, 573 → 595 — LUMO (β) =573, HOMO (β) =572	T_{P+V}
	4. 381 nm — $Peak_3$	4. 0.45804(β)	571 → 577	T_V
-3	1. 627 nm — $Peak_1$	1. 0.41972(α), 0.46834(α)	573 → 582, 575 → 586 — LUMO (α) =576	T_P
	2. 464 nm, 3. 456 nm — $Peak_2$	2. 0.38029(α), 0.59251(β) 3. 0.34293 (α), 0.30207 (α), 0.48134(β)	571 → 576, 571 → 573 575 → 577, 570 → 577, 570 → 574 — HOMO (α) =575, LUMO (β) =573	T_V
	4. 409 nm — $Peak_3$	4. 0.39015(β)	572 → 575 — HOMO (β) =572	T_V
-4	1. 627 nm — $Peak_1$	1. 0.51075(α)	573 → 583 — HOMO (α) =577, LUMO (α) =576	T_P
	2. 461&450nm — $Peak_2$	2. 0.34758(α), 0.58646(β) & 0.58164(α)	570 → 577, 570 → 573, 576 → 589 — LUMO (β) =573	T_{P+V}
	3. 403 nm — $Peak_3$	3. 0.12102(α) , 0.29542(β)	572 → 601, 572 → 574 — HOMO (β) =572	T_{P+V}
-5	1. 628 nm — $Peak_1$	1. 0.56693(α), 0.31512(α)	573 → 582, 575 → 583 — LUMO (α) =578	T_P
	2. 447 nm — $Peak_2$	2. 0.42940(α), 0.19122 (β)	573 → 587, 564 → 573 — HOMO (α) =577	T_{P+V}
	3. 407 nm — $Peak_3$	3. 0.10475(α), 0.28666(β)	562 → 579, 572 → 573 — LUMO (β) =573	T_{P+V}
	4. 360 nm — $Peak_4$	4. 0.29656(α), 0.37724(β)	575 → 578, 572 → 578 — HOMO (β) =572	T_V
-6	1. 627 nm — $Peak_1$	1. 0.55921(α), 0.38163(β)	574 → 583, 572 → 585 — LUMO (α) =578	T_P
	2. 503 nm — $Peak_2$	2. 0.31071(α), 0.39079(α), 0.58423(β)	577 → 589, 577 → 590, 573 → 586 — HOMO (α) =577	T_{BP}
	3. 447 nm, 4. 444 nm — $Peak_3$	3. 0.37777(α), 0.30295(α), 0.15578(β) 4. 0.47423(α), 0.30820(α) , 0.13499(β)	574 → 581, 576 → 588, 566 → 576 573 → 587, 573 → 589, 565 → 575 — LUMO (β) =574, HOMO (β) =573	T_{P+V}
	5. 404 nm — $Peak_4$	0.38954(β), 0.22198(β)	571 → 574, 577 → 589	T_V
-10	1. 527 nm, 2. 519 nm — $Peak_1$	0.32824, 0.29434 0.21182, 0.20778, 0.21359	573 → 582, 577 → 578 573 → 583, 574 → 583, 576 → 585 — HOMO =578	T_{BP}
	3. 423 nm, 4. 411 nm — $Peak_2$	0.24788 0.31028	577 → 578, 577 → 586 573 → 578, 571 → 574 — LUMO = 577	T_{BP}
	5. 355 nm, 6. 345 nm — $Peak_3$	0.22883 0.20108, 0.23104	577 → 574, 571 → 574 569 → 551, 571 → 581	T_{P+V}

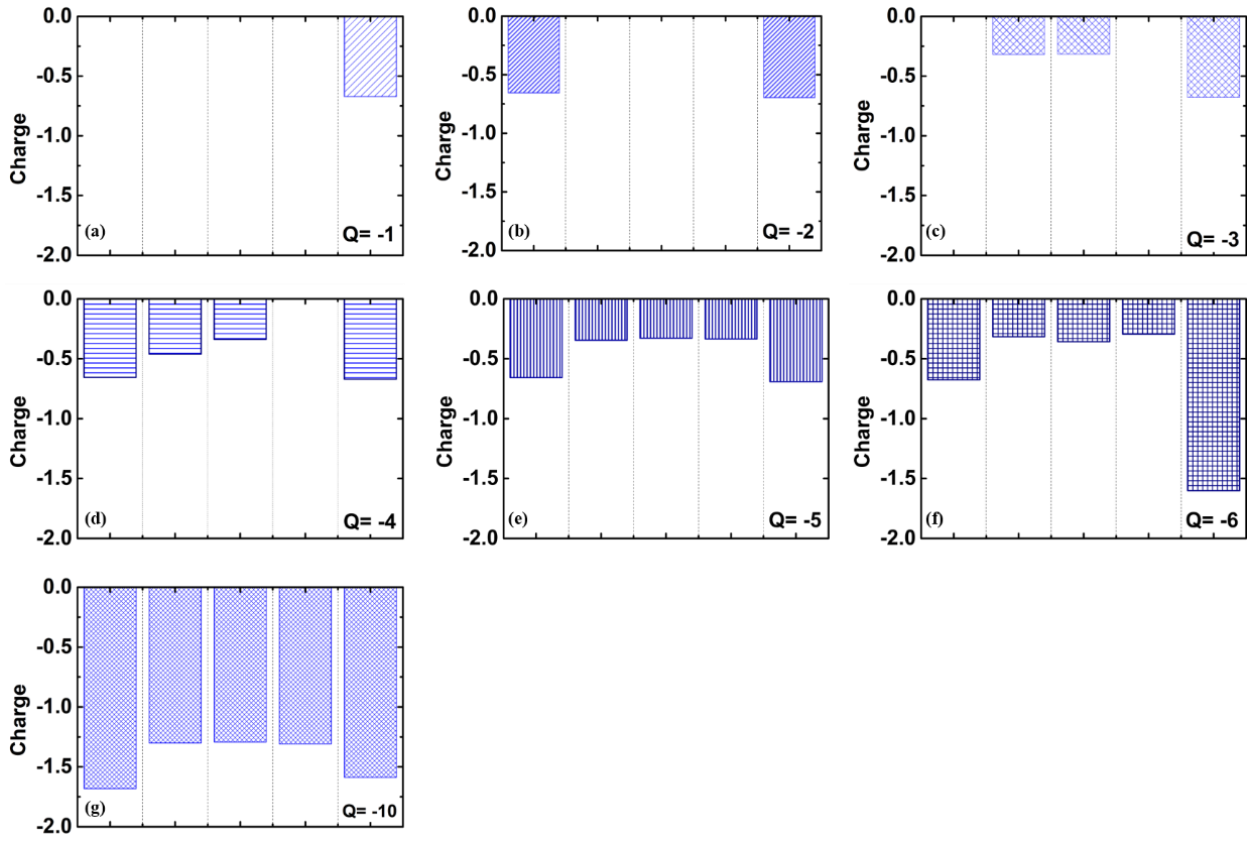

Figure S15: The charge distribution on different NDI-units in solvent phase within the NDI-TVT polymer chain showing distinct distribution of charge at various doped levels from Q= -1 to -6 and -10 in solvent phase.

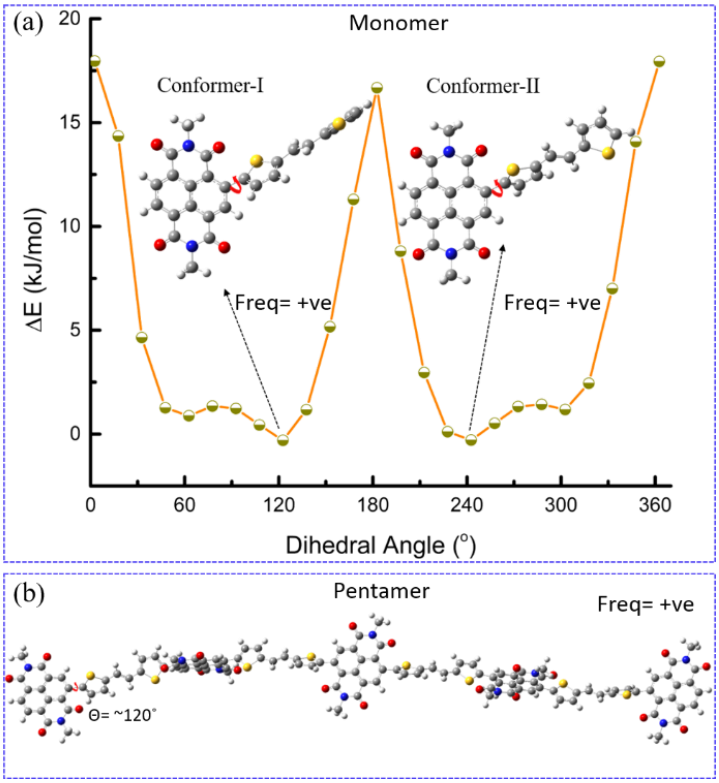

Figure S16: (a) Potential energy surface (PES) scan of the dihedral angles between the NDI and TVT moieties, θ of one DFT-optimized NDI-TVT monomer along with the computed frequency for the two lowest-energy conformers, namely, Conformer-I and Conformer-II, performed at the same level of theory to the DFT calculation. (b) The computed frequency of the lowest energy conformer, Conformer-I, θ=120° of the pentamer NDI-TVT. No imaginary frequency indicates that the conformer is the global minimum on the potential energy surface.

We have performed a thorough conformational analysis through a potential energy surface (PES) scan of the dihedral angles between the NDI and TVT moieties on the monomer unit of the co-polymer NDI-TVT to check the presence of any other energetically closed conformers. Figure S16(a) shows that two conformers, namely, Conformer-I and Conformer-II, where the dihedral angles between the NDI moiety and TVT moiety, θ are ~120° and ~240° have the lower energy, and the conformer-I (θ=~120°) is the lowest on the PES. In the conformation of 5-unit NDI-TVT that we have considered as the model system in our study, the dihedral angle between each NDI and TVT is ~120°, representing that the selected structure is energetically favorable. Furthermore, we have performed a vibrational frequency analysis of the lowest energy conformer for the monomer and pentamer neutral chains as well as for a highly doped chain (C_{red}= 200%) to verify the stationary points as global minima (zero imaginary frequency). We found there are no imaginary frequencies that correspond to the global minima on the PES

and indicate that the conformer of NDI-TVT we have considered is the energetically favorable stable structure.

Accuracy of 6-31+G(d) basis set in Calculating Structural, Electronic, and Optical Properties of NDI-TVT:

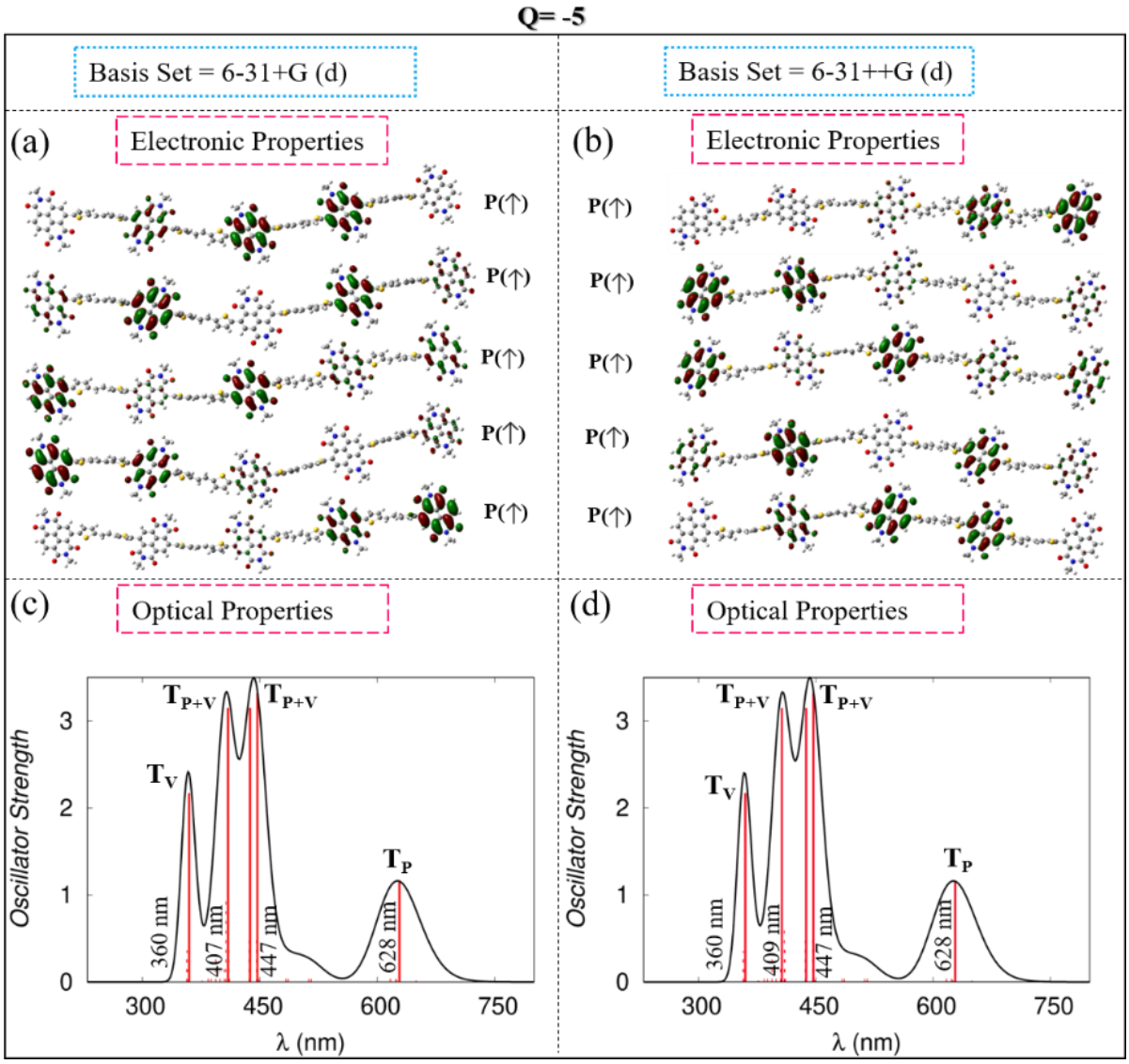

Figure S17: [Upper panel] The electronic properties of the charged state Q = -5, calculated using two different basis sets, (a) 6-31+G(d) (the basis set considered in the present study) and (b) 6-31++G(d). [Lower panel] Optical properties of the charged state Q = -5 using two basis sets, (c) 6-31+G(d) and (d) 6-31++G(d).

We have performed the effect of the basis set in predicting the structural, electronic, and optical properties of NDI-TVT polymer by considering three different basis sets, 3-21+G, 6-31+G(d),

and 6-311+G(d). The electronic and optical properties of doped NDI-TVT calculated using the basis set, 6-31++G(d) that includes diffuse functions on all atoms, including hydrogen, are almost the same as that of the basis set 6-31+G(d), where the diffuse functions are only on the heavy atoms, and we observe the molecular orbitals are localized only on the heavy atoms, see Figure S17. Furthermore, we have compared the 6-31+G(d) basis set used in our present study with both a higher (6-311+G(d)) and a lower (3-21+G) basis set, see Figure S18. For the charged state Q = -6, the structural, electronic, and optical properties obtained with the 6-31+G(d) basis set were nearly identical to those from the higher basis set, 6-311+G(d). In contrast, we observed significant differences in the structural, electronic, and optical properties when using the lower basis set, 3-21+G, indicating that it is not a reliable model for predicting the structural, electronic, and optical properties of NDI-TVT.

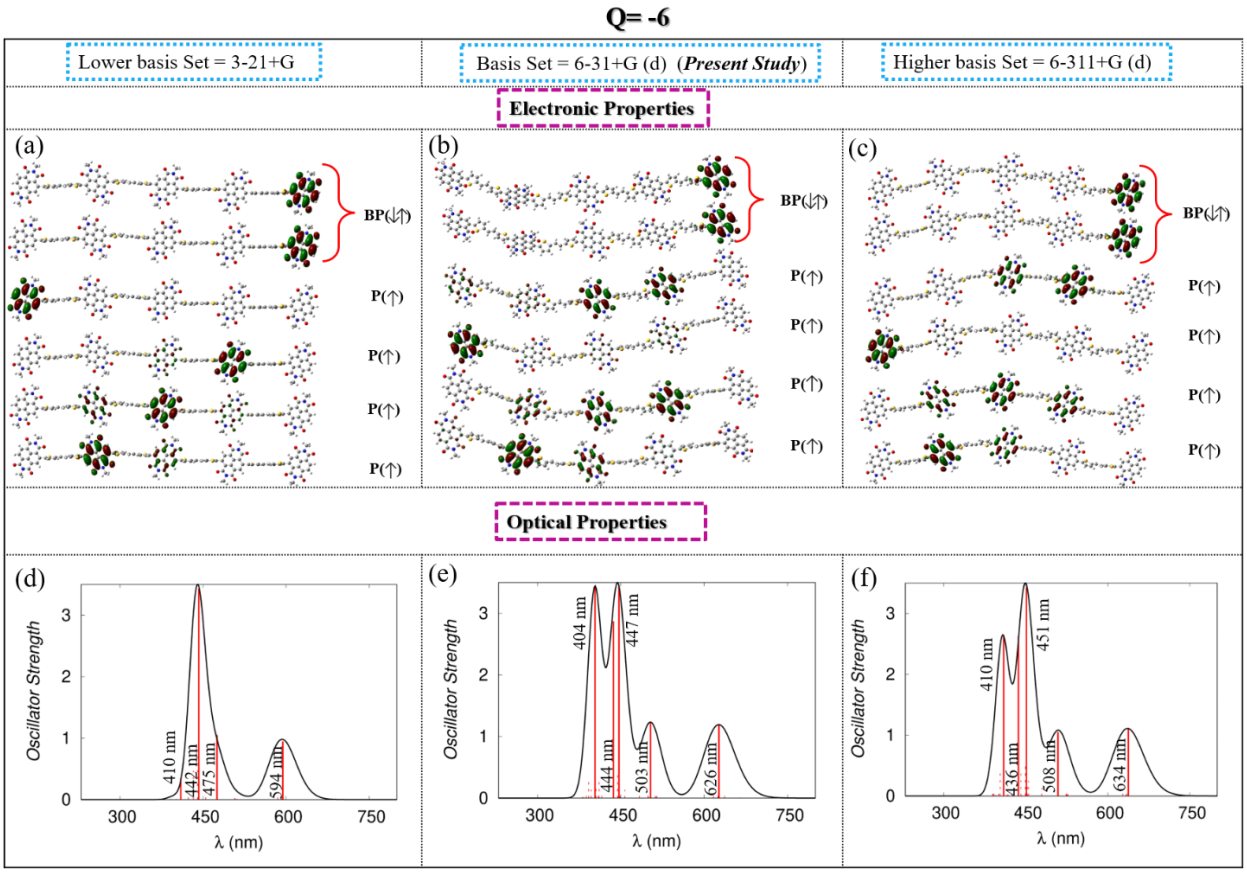

Figure S18: **Upper panel:** The electronic properties of the charged state Q = -6 calculated using (a) lower basis sets, 3-21+G, (b) 6-31+G (d) (present study), and (c) higher basis set 6-311+G (d). **Lower panel:** Optical properties of the charged state Q = -6 calculated using (d) lower basis sets, 3-21+G, (e) 6-31+G (d) (present study), and (f) higher basis set 6-311+G (d).

Broken-Symmetry Calculation of Q=-2, spin state S=0:

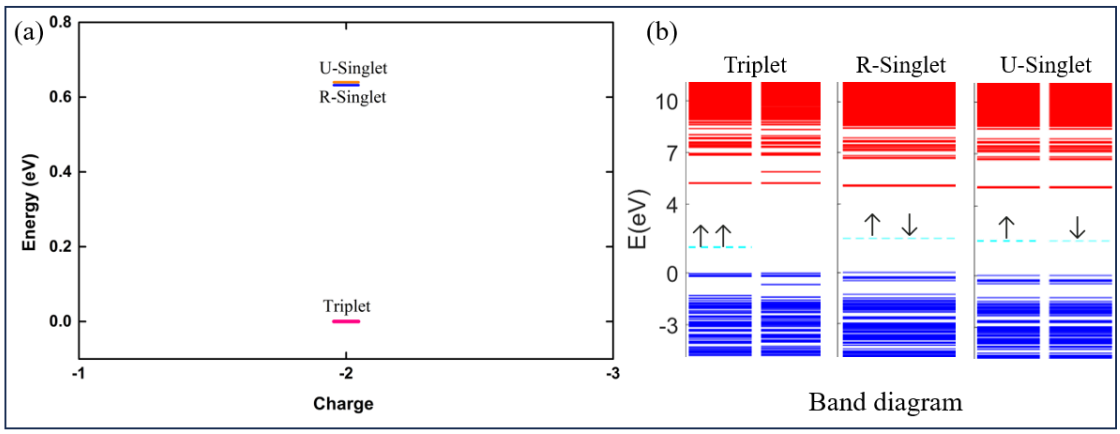

Figure S19: (a) Energy diagram of Q=-2 for the open shell calculation of Triplet (S=1) and U-Singlet (S=0) state and closed shell calculation of R-Singlet state. (b) Band diagram of Triplet, R-Singlet, and U-Singlet state.

Using a broken symmetry approach, we have performed the open-shell DFT calculation for the singlet spin state S=0. From the energy diagram Figure S19(a), we note that the open-shell singlet state calculation, i.e., U-Singlet using broken symmetry, has equivalent energy compared to the closed-shell singlet state calculation, i.e., R-Singlet, and both converge at higher energy compared to the open-shell triplet spin-state calculation (S=1). It is noteworthy that for the singlet state (S=0), U-Singlet calculation converges to the spin-degenerate energy band diagram, i.e., identical to the results obtained for the case of the R-DFT, see Figure S19(a).

π→π* Electronic Transition of Q=0 in Absorption Spectra:

In the donor-acceptor polymer (NDI-TVT) system for the neutral polymer, two types of transition are shown, i.e., π→π* transition and an ICT (intramolecular charge transfer) transition[6–8]. The peak at 343 nm originates from three transitions, one from HOMO-2 to LUMO+5 and the second from HOMO to LUMO+7, and the third one from HOMO-12 to LUMO+2, see Figure S20. We have observed that both HOMOs and LUMOs participating in those transitions are largely located at the TVT units for the first two transitions, and they are mainly located at the NDI moieties for the third transition, see Figure S20.

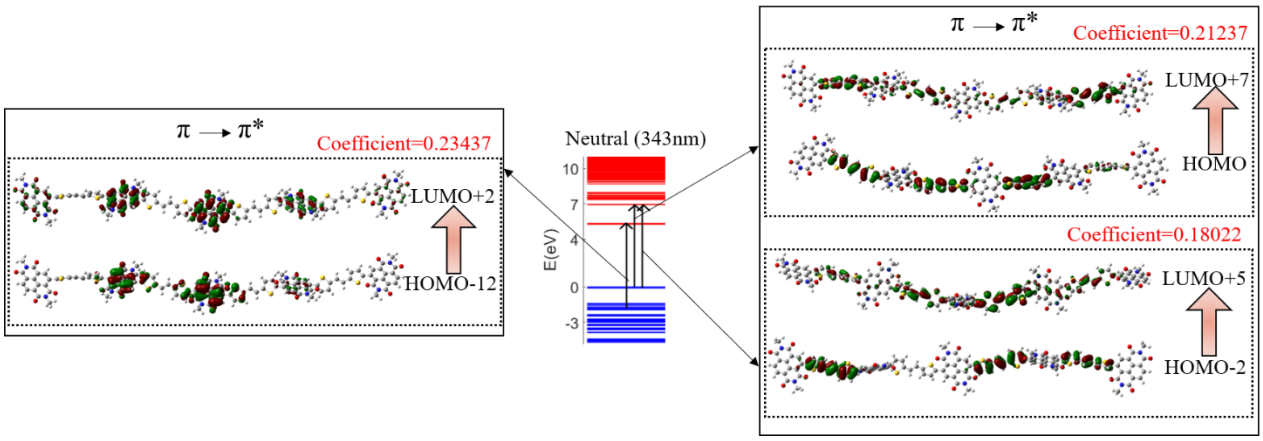

Figure S20: The molecular orbital distributions of HOMOs-LUMOs participating in the π→π* transition on the neutral NDI-TVT polymer in the solvent phase.

Effect of Chain Length in Predicting Electronic Structures of Reduced NDI-TVT:

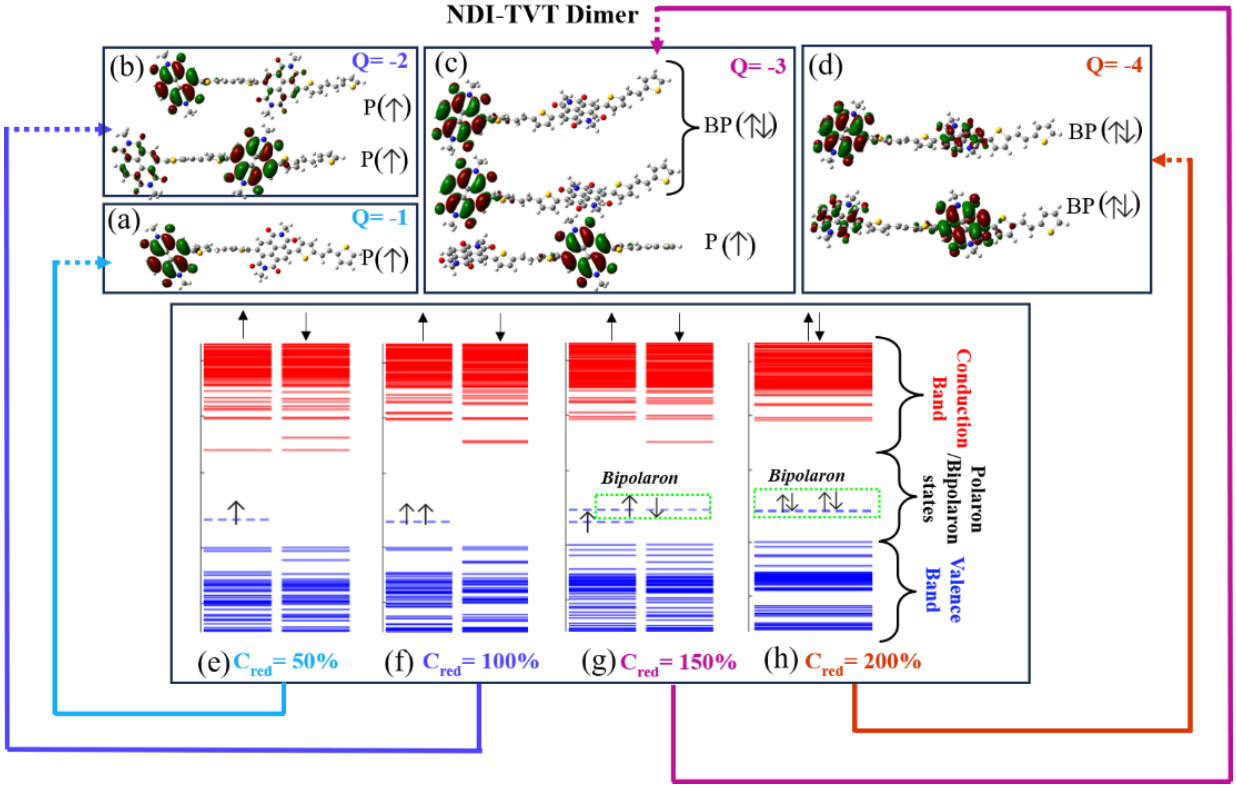

Figure S21. Molecular orbital diagrams of a NDI-TVT dimer at all reduction states, (a) Q=-1, Cred=50%, (b) Q=-2, Cred=100%, (c) Q=-3, Cred=150%, (d), Q=-4, Cred=200%, and the energy band diagrams of NDI-TVT dimer at all the reduction states, (e) Q=-1, Cred=50%, (f) Q=-2, Cred=100%, (g) Q=-3, Cred=150%, (h), Q=-4, Cred=200%.

We have done the analysis of the smaller unit of the NDI-TVT chain, viz., dimer, which shows that the bipolarons formation arises only beyond 100% doping of the polymer chain, see Figure

S21. This observation remains consistent with the longer chain (pentamer). As a result, we can conclude that the formation of the bipolarons only beyond a 100% reduction level is not an artifact of chain length.

Table.S3: Spin contamination values for open shell calculations of high spin multiplicities for charge states Q = -3 to -6 of NDI-TVT in the solvent phase.

Charges (Q)	Multiplicities of open shell calculations	Expectation values $<S^2>$	Spin (s)	s(s+1)	Spin contamination $< S^2 > - s(s+1)$
-3	Quartet	3.7525	1.5	3.75	0.0025
-4	Quintet	6.0037	2	6.00	0.0037
-5	Sextet	8.7549	2.5	8.75	0.0049
-6	Quintet	6.0037	2	6.00	0.0037

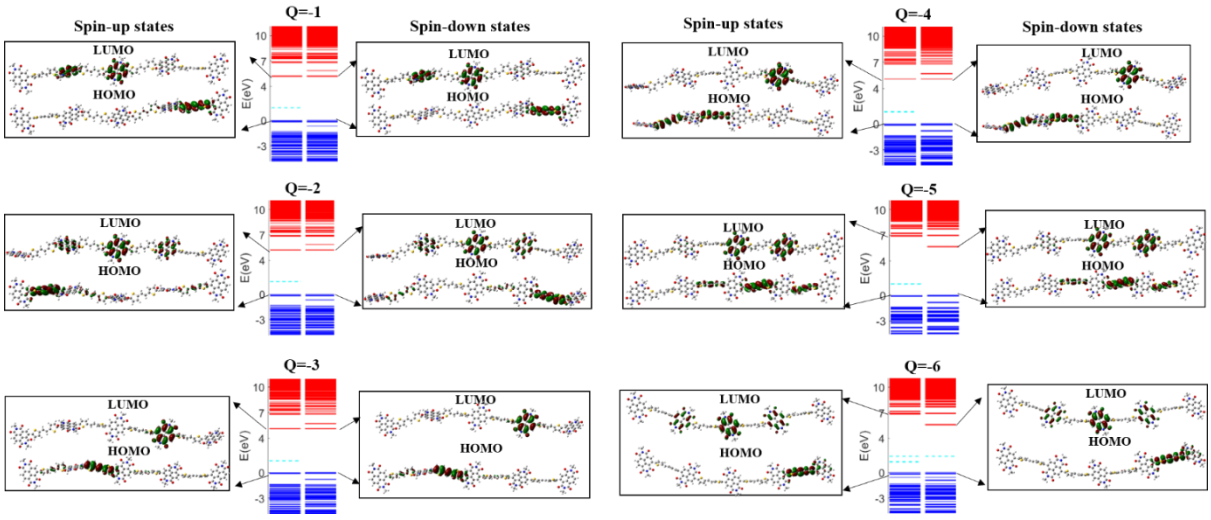

Figure S22: Band diagrams and molecular orbitals of HOMO (highest occupied molecular orbital) and LUMO (lowest unoccupied molecular orbital) of NDI-TVT polymer at different charged states, Q=-1 to -6, in the solvent phase.

References:

(1) Schlegel, H. B. Optimization of Equilibrium Geometries and Transition Structures. *J. Comput. Chem.* **1982**, *3* (2), 214–218. https://doi.org/10.1002/JCC.540030212.

(2) Ipatov, A.; Cordova, F.; Doriol, L. J.; Casida, M. E. Excited-State Spin-Contamination in Time-Dependent Density-Functional Theory for Molecules with Open-Shell Ground States. *J. Mol. Struct. THEOCHEM* **2009**, *914* (1–3), 60–73.

(3) Young, D. *Computational Chemistry: A Practical Guide for Applying Techniques to Real World Problems*; John Wiley & Sons, 2004.

(4) Kitsaras, M.-P.; Stopkowicz, S. Spin Contamination in MP2 and CC2, a Surprising Issue. *J. Chem. Phys.* **2021**, *154* (13).

(5) Zozoulenko, I.; Singh, A.; Singh, S. K.; Gueskine, V.; Crispin, X.; Berggren, M. Polarons, Bipolarons, And Absorption Spectroscopy of PEDOT. *ACS Appl. Polym. Mater.* **2019**, *1* (1), 83–94. https://doi.org/10.1021/acsapm.8b00061.

(6) Roy, P.; Jha, A.; Yasarapudi, V. B.; Ram, T.; Puttaraju, B.; Patil, S.; Dasgupta, J. Ultrafast Bridge Planarization in Donor-π-Acceptor Copolymers Drives Intramolecular Charge Transfer. *Nat. Commun. 2017 81* **2017**, *8* (1), 1–10. https://doi.org/10.1038/s41467-017-01928-z.

(7) Kim, R.; Amegadze, P. S. K.; Kang, I.; Yun, H.; Noh, Y.; Kwon, S.; Kim, Y. High-mobility Air-stable Naphthalene Diimide-based Copolymer Containing Extended Π-conjugation for N-channel Organic Field Effect Transistors. *Adv. Funct. Mater.* **2013**, *23* (46), 5719–5727.

(8) Caironi, M.; Bird, M.; Fazzi, D.; Chen, Z.; Di Pietro, R.; Newman, C.; Facchetti, A.; Sirringhaus, H. Very Low Degree of Energetic Disorder as the Origin of High Mobility in an N-Channel Polymer Semiconductor. *Adv. Funct. Mater.* **2011**, *21* (17), 3371–3381. https://doi.org/10.1002/ADFM.201100592.